10-18-2013

Depth-Dependent Resistance of Granular Media to Vertical Penetration

Theodore A. Brzinski III
University of Pennsylvania

Patrick Mayor
University of Pennsylvania

Douglas J. Durian
University of Pennsylvania, djdurian@physics.upenn.edu

Depth-Dependent Resistance of Granular Media to Vertical Penetration

Abstract

We measure the quasistatic friction force acting on intruders moving downwards into a granular medium. By utilizing different intruder geometries, we demonstrate that the force acts locally normal to the intruder surface. By altering the hydrostatic loading of grain contacts by a sub-fluidizing airflow through the bed, we demonstrate that the relevant frictional contacts are loaded by gravity rather than by the motion of the intruder itself. Lastly, by measuring the final penetration depth versus airspeed and using an earlier result for inertial drag, we demonstrate that the same quasistatic friction force acts during impact. Altogether this force is set by a friction coefficient, hydrostatic pressure, projectile size and shape, and a dimensionless proportionality constant. The latter is the same in nearly all experiments, and is surprisingly greater than one.

Disciplines

Physical Sciences and Mathematics | Physics

Depth-Dependent Resistance of Granular Media to Vertical Penetration

T. A. Brzinski III, P. Mayor, and D. J. Durian

Department of Physics and Astronomy, University of Pennsylvania, Philadelphia, Pennsylvania 19104, USA
(Received 17 July 2013; published 18 October 2013; corrected 30 January 2014)

We measure the quasistatic friction force acting on intruders moving downwards into a granular medium. By utilizing different intruder geometries, we demonstrate that the force acts locally normal to the intruder surface. By altering the hydrostatic loading of grain contacts by a sub-fluidizing airflow through the bed, we demonstrate that the relevant frictional contacts are loaded by gravity rather than by the motion of the intruder itself. Lastly, by measuring the final penetration depth versus airspeed and using an earlier result for inertial drag, we demonstrate that the same quasistatic friction force acts during impact. Altogether this force is set by a friction coefficient, hydrostatic pressure, projectile size and shape, and a dimensionless proportionality constant. The latter is the same in nearly all experiments, and is surprisingly greater than one.

The flow of granular systems defies rheological description, in part because shear tends to localize and conventional instruments cannot measure stress and strain [1]. An alternative approach is to measure the force on a moving intruder [2–11]. For slow horizontal motion at a fixed depth, the force is rate independent and proportional to both the projected area of the intruder and its depth; this is due to friction acting at gravity-loaded contacts [3,7]. For a sphere dropped vertically onto a granular medium, the depth-averaged stopping force, deduced by $\langle F \rangle = mgH/d$ where H is the total drop distance and d is the penetration depth, can be much greater [4]. Most impact behavior can be reconciled by an equation of motion of the form [12,13]

$$ma = -mg + F(z) + bv^2. \qquad (1)$$

Here $F(z)$ is a rate-independent friction that grows with depth z, and bv^2 is an inertial drag proportional to the square of projectile speed v, due to momentum transfer just as for a fluid a high Reynolds number. Reference [7] showed that the stopping force experienced by a horizontally rotating rod is of the same form, but smaller in magnitude, and that $F(z)$ grows with depth due to gravitational loading of frictional contacts. References [14,15] explored the role of air and grain packing fraction. Reference [16] demonstrated that $F(z)$ increases monotonically with the prestressing of the packing normal to the direction of gravity. Reference [17] suggested the existence of an additional constant force term F_0, finding that both F_0 and b increase with projectile size. Reference [18] demonstrated that $F(z)$ saturates with Janssen-like z dependence for deep impacts. In the absence of wall effects [18–20], the typical assumed form is $F(z) = kz$, dating back to Ref. [21].

Here we address two outstanding issues with regards to the $F(z)$ friction term in Eq. (1). First, while the total stopping force points up, the extent to which friction acts locally normal versus tangential to surface area elements of the projectile is not known. Second, while $F(z)$ has been shown to grow with gravitational loading of the bed [22,23], it is unknown how the motion loading of contacts by the intruder affects the total stopping force. In particular, force chains extend from the projectile deep into the medium and are intermittently loaded and broken during impact [17,24–26]; this could contribute to friction. Our approach is to directly measure $F(z)$ under two sets of conditions. In one we vary the shape of the projectile in order to alter the fraction of the projectile surface that moves parallel vs perpendicular to the medium. In the other, we impose a subfluidizing upflow of air to systematically counteract the gravitational loading of the grains without affecting their motion loading. One might expect friction between grains and projectile to act tangential to their surface of contact and to be stronger due to the additional motion loading. In striking contrast, we find the local friction force to be

$$d\mathbf{F} = \alpha\mu(\rho g z)d\mathbf{A}, \qquad (2)$$

where μ is an internal friction coefficient equal to the tangent of the repose angle, $\rho g z$ is the gravitational loading pressure, $d\mathbf{A}$ is an infinitesimal area element pointing normal to the projectile surface, and $\alpha = 35 \pm 5$ is a number we measure to be the same in nearly all experiments. The total drag force is found by integrating over $d\mathbf{A}$. Such behavior is relevant for locomotion in and on grains [27], as well as for meteorite strikes [11,21,28].

Our granular medium consists of cohesionless glass spheres of diameter range $300 \pm 50\ \mu m$, bulk density $\rho = 1.48\ g/cm^3$, and draining angle of repose $22°$, giving $\mu = 0.40$. The grains fill a 19-cm-diameter acrylic cylinder to a depth of 20 cm; this is large enough to avoid wall effects [19,20]. Underneath is an apparatus for applying a uniform upflow of air through the granular packing as in Refs. [7,13]. Before each experiment the

grains are first fluidized and the upflow is then gradually
stopped, giving a level surface and a packing fraction of
$\varphi = 0.59$.

In the first set of experiments, a projectile is hung from a
force gauge suspended beneath a pulley. The projectiles
are cylindrical, with radii R between 0.476 and 3.85 cm,
conical, with apex half-angles ϕ of 15, 30, 45, and 60
degrees, and spherical, with radii R of 1.27, 2.54, and
5.05 cm. The pulley is used to slowly increase the fraction
of the projectile's weight that is supported by the granular
media. The depth, z, of the bottom of the projectile is
deduced with a height gauge, and a simultaneous reading
of the force gauge is recorded. Initially we observe a
single-valued force for each depth; however, below a short
initial penetration depth we observe stick-slip behavior.
In this case, the penetration depth remains constant while
the load increases. Beyond about 20% [29], the granular
material fails, and the projectile falls a short distance.
Because $F(z)$ is the rate-independent drag acting on a
moving intruder, we consider only the forces at which
the material fails.

Results for $F(z)$ are plotted against z for fifteen
intruders of various sizes and shapes. We normalize
according to expectation given by integrating Eq. (2)
with $d\mathbf{A}$ pointing normal to the surface area elements of
the intruder [29]:

$$\frac{F(z)}{\alpha\mu\rho g} \begin{cases} \pi R^2 z & \text{cylinder} & (3a) \\ (\pi/3)\tan^2\phi\, z^3 & \text{cone} & (3b) \\ \pi(R - z/3)z^2 & \text{sphere}, z \leq R & (3c) \\ \pi(z - R/3)R^2 & \text{sphere}, z \geq R & (3d) \end{cases} \qquad (3)$$

If $d\mathbf{A}$ points tangential to the area elements, the scaling is
quite different: Rz^2 for cylinders, $\tan\phi z^3$ for cones, and
$(z - 0.58R)R^2$ for spheres at $z > R$ [29]. Thus we plot
(a) $F(z)/R^2$ vs z for cylinders, (b) $F(z)/\tan^2\phi$ vs z for
cones, and (c) $F(z)/R^3$ vs z/R for spheres. Indeed, in
accord with Eq. (3) this causes excellent collapse.

As a further test, beyond collapse, we compare force
data with the expected forms. In Figs. 1(a) and 1(b) for
cylinders and cones, the best-fit power laws have respective
exponents of 1.06 ± 0.06 and 2.95 ± 0.36, consistent with
a normal direction for $d\mathbf{A}$. In Fig. 1(c) for spheres, the data
at $z > R$ fall on a line proportional to $z/R - 1/3$, consis-
tent with (d) in Eq. (3) as opposed to the surface-tangent
expectation of $z/R - 0.58$ [29]. For $z < R$ the data are
also fit well by (c) in Eq. (3). Altogether, the agreement
between data and Eq. (3) demonstrates that the quasistatic
friction force acts primarily normal to the area elements of
the intruder. In principle, it ought to act tangential, too, but
this effect is much smaller.

Next, in order to distinguish the respective roles
of gravity-loaded and motion-loaded contacts, we subject
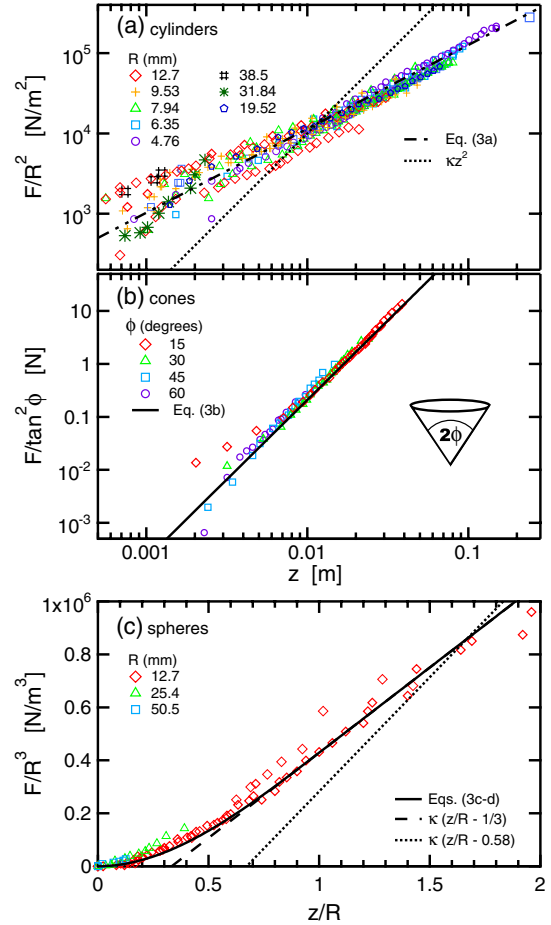the system to a subfluidizing flow of air. Since the airspeed

FIG. 1 (color online). Friction force versus depth for
(a) cylindrical, (b) conical, and (c) spherical intruders of differ-
ent geometry; R is radius and ϕ is apex half-angle. The scaling
of the y axes, and the curves through the data, are the expecta-
tions of Eq. (3) for $d\mathbf{F}$ normal to the intruder surface area
elements. The dashed (dotted) line in (c) represents expectation
for $z > R$ for $d\mathbf{F}$ normal (tangential) to the intruder.

U is proportional to the gradient in air pressure across
the sample, this modifies the effective hydrostatic pres-
sure gradient as $\rho g \to \rho g(1 - U/U_c)$, where U_c is the
fluidization airspeed where the upflow exactly balances
gravity. Thus, without actually changing gravitational ac-
celeration [10,22,23], the effective gravity loading is
reduced by a subfluidizing upflow, $0 < U < U_c$, similarly,
it is enhanced by a downflow, $U < 0$. The motion loading
of contacts, and the inertial drag force, ought not be
affected by airflow. Note, too, that the very presence of
air does not affect the impact behavior since the grains are
sufficiently large [13]. Furthermore, even for smaller
grains, air effects vanish near $\varphi = 0.58$ [15], which is
just below the conditions here of $\varphi = 0.59$.

For sample preparation, we begin as usual but then
gradually tune the airspeed to a value in the range
$U < U_c$. Downflow, $U < 0$, is achieved by connecting
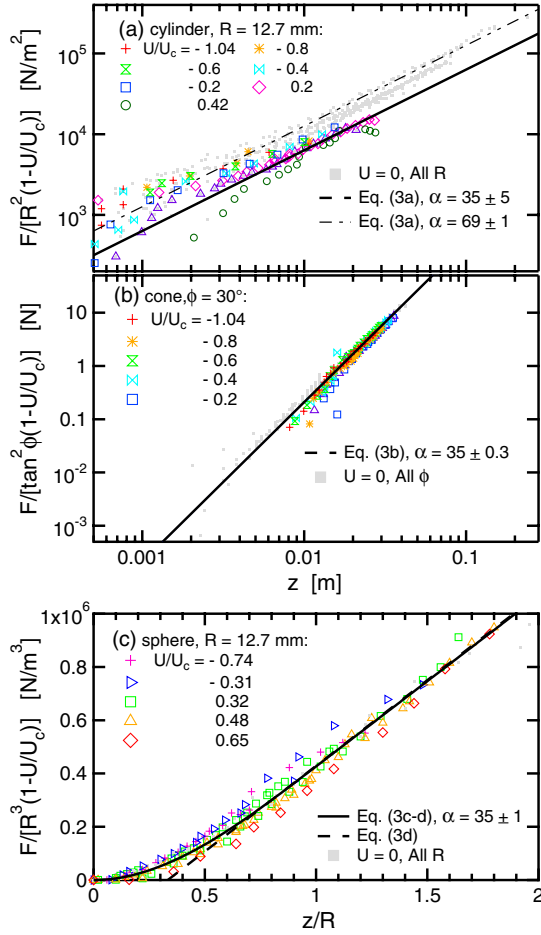the apparatus to a Shop-Vac. The rate-independent

FIG. 2 (color online). Friction force versus depth for
(a) cylindrical, (b) conical, and (c) spherical probes, normalized
as in Fig. 1 and also by $1 - U/U_c$, where U is airspeed and U_c is
airspeed at fluidization. The solid curves are simultaneous fits to
Eq. (3) with $\alpha = 35 \pm 5$. All data from Fig. 1 are replotted as
small grey points.

frictional drag, $F(z)$, is then measured as above. The results
are scaled by geometrical factors, as well as by
$(1 - U/U_c)$, and plotted in Fig. 2. For comparison, all
data from Fig. 1 are included as grey squares. Again this
normalization causes good collapse, and all the data dem-
onstrate the same scaling as the data for $U = 0$ presented
in Fig. 1: $F(z)/(1 - U/U_c)$ is proportional to $R^2 z$ for
cylinders, to $\tan^2 \phi z^3$ for cones, and is consistent with
(c) and (d) in Eq. (3) for spheres.

The fits in Figs. 2(a)–2(c) to Eq. (3) are made using only
one dimensionless parameter: $\alpha = 35 \pm 5$. This value is
close to $\alpha = 26 \pm 3$, as measured in [13] for vertically
impacting spheres at $U = 0$, hinting that α may have a
universal value close to 30 for vertical impacts onto cohe-
sionless granular materials. Between the quality of data
collapse, the agreement between data and Eq. (3), and the
universality of the constant α for vertical impacts, we've
demonstrated that the entirety of the effect of a subfluid-
izing flow of air through the sample is captured by the

reduction factor $(1 - U/U_c)$. Thus the magnitude of $F(z)$
must be determined by gravity-loaded contacts in the bed,
and not by contacts loaded via projectile motion.

As an aside, cylindrical projectiles in the absence
of gas flow prove to be somewhat of a special case.
The fit of (a) in Eq. (3) to the cylinder data in Fig. 1(a)
gave $\alpha = 70$ and is replotted as a dash-dotted line in Fig. 2.
So while the drag on cylinders exhibits radius and depth
dependence consistent with (a) in Eq. (3), it is double the
magnitude of any other geometry in our quasistatic low-
ering experiments. This is discussed further in [29].

One might expect the motion loading to be more rele-
vant for a projectile at $v \neq 0$. In order to demonstrate that
the behavior for quasistatic lowering is also valid more
generally, we conduct several conventional impact experi-
ments utilizing cylindrical and spherical projectiles. Each
projectile is equipped with a small square rod, capped with
a ferrous metal tip, to suspend the projectile from an
electromagnet. We measure the height of the projectile
above the granular surface, h, turn off the electromagnet,
allow the projectile to free-fall onto the granular medium,
and measure d via height gauge. We repeat this procedure
for a range of subfluidizing up- and downflows of air to
determine d as a function of the normalized gas speed,
U/U_c.

The results for d vs U/U_c, plotted in Fig. 3, conform to
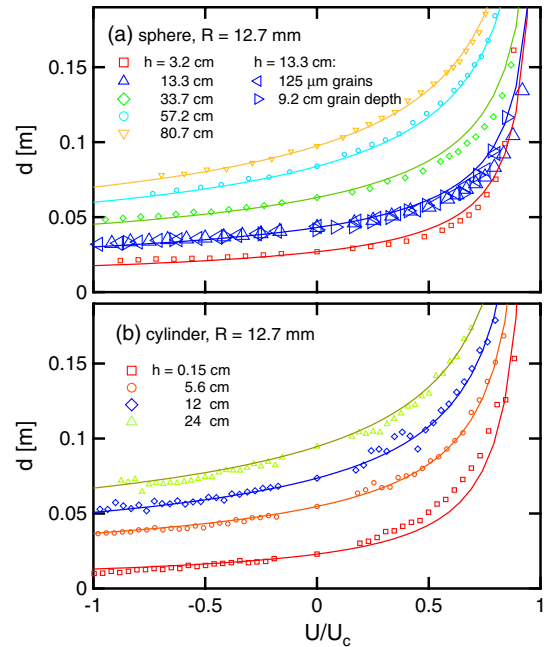intuition. As $U \to U_c$, d increases without apparent bound,

FIG. 3 (color online). Penetration depth versus normalized
airspeed for (a) a sphere of mass 0.07 kg and (b) a cylinder of
mass 0.2 kg, from various drop heights h. The grains are 300 μm
and the packings are 19.4 cm deep, except for two special cases
in (a) where the depth and the grain size are decreased. The
curves represent solutions of Eq. (2) and (a) in Eq. (3) with $\alpha =
35$, taking b to match the data at $U = 0$.

and as U becomes negative, d decreases monotonically. As a crucial check, penetration depths of the 12.7-mm-radius sphere for three different granular packings are shown in (a) by large blue triangles pointing up for usual conditions, pointing right for half the usual filling height, and hence half the imposed air pressure, and pointing left for smaller grains and hence a smaller U_c. Despite the different conditions, the three data sets are indistinguishable. This demonstrates the absence of both grain-size effects as well as interstitial air effects associated with packing fraction changes [14,15]. Thus, the up- or downflow of air serves only to modify the gravity loading of contacts.

Lastly we compare the measured final penetration depths with the exact solution of Eq. (1), calculated in [29]. For this, the initial impact speed is taken as $v = \sqrt{2gh}$, $F(z)$ is taken by (a) in Eq. (3) with $\alpha = 35$, and b is adjusted so that the prediction exactly matches the data at $U = 0$. The resulting predictions, shown as solid curves of Fig. 3, closely match the data for the entire range of airspeeds. This demonstrates that the same rate-independent friction force acts during impact as during quasistatic lowering.

To conclude, the decoupling of frictional and inertial drag forces in Eq. (1), seen earlier for horizontal motion [7], also holds for downward motion. The rate-independent upward friction term, $F(z)$, arises from local forces $d\mathbf{F}$ according to Eq. (2) that point normal to the intruder surface elements and that grow in proportion to a friction coefficient, gravitational hydrostatic pressure, and area. While we varied the hydrostatic pressure via depth and airflow, and we varied area elements via intruder size and shape, we did not vary the friction coefficient. However, its presence is intuitive and is supported by other work [30]. It is surprising that friction does not act at motion-loaded contacts or have a significant component tangential to the intruder. The latter can be judged somewhat just by plunging your finger into a container of grains. This suggests that intruder roughness and tangential grain flow are not crucial, which is consistent with the observation that slick and tacky intruders have the same penetration depths [4]. This could be tested directly by roughening the intruder and imaging grain dynamics either for disks [17,24,26] or index-matched grains [16].

Another surprise is that the numerical coefficient in Eq. (2) is so large. It is nice that $\alpha = 35 \pm 5$ holds for nearly all data, but a number of order 1 would have been expected for ordinary Coulomb friction acting between grains and intruder. Evidently, the relevant gravity-loaded contacts comprise a greater area and hence must be spread throughout a volume of grains near the intruder. We propose a physical picture, based on force chains that extend from the intruder into the medium [17,24–26]. These can be loaded statically and dynamically, and preferentially radiate away momentum [17,26]. They also tend to be oriented normal to the projectile and to exist in a background sea of gravity-loaded grains. Rigid-body motion of entire force chains could thus mobilize a large volume of gravity-loaded frictional grain-grain contacts and give rise to a normal $d\mathbf{F}$ and $\alpha \gg 1$. In effect, the chains are loaded between opposing forces from the intruder and from the surrounding gravity-loaded grains. Perhaps this may also be thought of as a form of dynamical heterogeneity [31], whereby flow is accomplished by intermittently excited subpopulations of mobile and immobile grains. Such an analogy correctly suggests that at very high intruder speeds, where grains are fluidized far from jamming, the stopping force is dominated by inertial effects, and vice versa for very low intruder speeds.

[1] H. M. Jaeger, S. R. Nagel, and R. P. Behringer, Rev. Mod. Phys. **68**, 1259 (1996).

[2] R. Albert, M. A. Pfeifer, A.-L. Barabási, and P. Schiffer, Phys. Rev. Lett. **82**, 205 (1999).

[3] I. Albert, P. Tegzes, R. Albert, J. Sample, A.-L. Barabási, T. Vicsek, B. Kahng, and P. Schiffer, Phys. Rev. E **64**, 031307 (2001).

[4] J. S. Uehara, M. A. Ambroso, R. P. Ojha, and D. J. Durian, Phys. Rev. Lett. **90**, 194301 (2003).

[5] G. Hill, S. Yeung, and S. A. Koehler, Europhys. Lett. **72**, 137 (2005).

[6] J. Geng and R. P. Behringer, Phys. Rev. E **71**, 011302 (2005).

[7] T. A. Brzinski, III. and D. J. Durian, Soft Matter **6**, 3038 (2010).

[8] N. Gravish, P. B. Umbanhowar, and D. I. Goldman, Phys. Rev. Lett. **105**, 128301 (2010).

[9] Y. Takehara, S. Fujimoto, and K. Okumura, Europhys. Lett. **92**, 44 003 (2010).

[10] D. J. Costantino, J. Bartell, K. Scheidler, and P. Schiffer, Phys. Rev. E **83**, 011305 (2011).

[11] J. C. Ruiz-Suárez, Rep. Prog. Phys. **76**, 066601 (2013).

[12] L. S. Tsimring and D. Volfson, Powders and Grains **2**, 1215 (2005).

[13] H. Katsuragi and D. J. Durian, Nat. Phys. **3**, 420 (2007).

[14] P. Umbanhowar and D. I. Goldman, Phys. Rev. E **82**, 010301 (2010).

[15] J. R. Royer, B. Conyers, E. I. Corwin, P. J. Eng, and H. M. Jaeger, Europhys. Lett. **93**, 28 008 (2011).

[16] K. N. Nordstrom, E. Lim, M. Harrington, and W. Losert, arXiv:1304.6419.

[17] A. H. Clark, L. Kondic, and R. P. Behringer, Phys. Rev. Lett. **109**, 238302 (2012).

[18] F. Pacheco-Vázquez, G. A. Caballero-Robledo, J. M. Solano-Altamirano, E. Altshuler, A. J. Batista-Leyva, and J. C. Ruiz-Suárez, Phys. Rev. Lett. **106**, 218001 (2011).

[19] E. L. Nelson, H. Katsuragi, P. Mayor, and D. J. Durian, Phys. Rev. Lett. **101**, 068001 (2008).

[20] A. Seguin, Y. Bertho, and P. Gondret, Phys. Rev. E **78**, 010301 (2008).

[21] D. Lohse, R. Rauhé, R. Bergmann, and D. van der Meer, Nature (London) **432**, 689 (2004).

[22] D. I. Goldman and P. Umbanhowar, Phys. Rev. E **77**, 021308 (2008).

[23] E. Altshuler, H. Torres, A. González-Pita, G. Sánchez-Colina, C. Pérez-Penichet, S. Waitukaitis, and R. C. Hidalgo, arXiv:1305.6796.

[24] K. E. Daniels, J. E. Coppock, and R. P. Behringer, Chaos **14**, S4 (2004).

[25] M. P. Ciamarra, A. Lara, A. Lee, D. Goldman, I. Vishik, and H. Swinney, Phys. Rev. Lett. **92**, 194301 (2004).

[26] A. H. Clark and R. P. Behringer, Europhys. Lett. **101**, 64001 (2013).

[27] C. Li, T. N. Zhang, and D. I. Goldman, Science **339**, 1408 (2013).

[28] A. M. Walsh, K. E. Holloway, P. Habdas, and J. R. deBruyn, Phys. Rev. Lett. **91**, 104301 (2003).

[29] See Supplemental Material http://link.aps.org/supplemental/10.1103/PhysRevLett.111.168002 for the calculation of total force acting on projectiles of various shapes for both normal and tangential friction, computation of impact dynamics, and extra experimental details.

[30] H. Katsuragi and D. J. Durian, Phys. Rev. E **87**, 052208 (2013).

[31] *Dynamical Heterogeneities in Glasses, Colloids, and Granular Media*, edited by L. Berthier, G. Biroli, J.-P. Bouchaud, L. Cipelletti, and W. van Saarloos (Oxford University Press, Oxford, 2011).